Effect of channel bed sediment on the transport behaviour of superparamagnetic silica encapsulated DNA microparticles in open channel injection experiments

Tang, Yuchen; van Rhijn, Fay; Abdelrady, Ahmed; Foppen, Jan Willem; Bogaard, Thom

DOI
10.1002/hyp.14962

Publication date
2023

Document Version
Final published version

Published in
Hydrological Processes

Received: 13 March 2023 | Revised: 31 July 2023 | Accepted: 1 August 2023

DOI: 10.1002/hyp.14962

RESEARCH ARTICLE

WILEY

Effect of channel bed sediment on the transport behaviour of superparamagnetic silica encapsulated DNA microparticles in open channel injection experiments

Yuchen Tang[1] | Fay van Rhijn[1] | Ahmed Abdelrady[2] | Jan Willem Foppen[1,3] | Thom Bogaard[1]

[1]Water Resources Section, Department of Civil Engineering and Geosciences, Delft University of Technology, Delft, The Netherlands

[2]European Centre of Excellence for Sustainable Water Technology, Leeuwarden, The Netherlands

[3]IHE Delft Institute for Water Education, Delft, The Netherlands

Correspondence
Yuchen Tang, Water Resources Section, Department of Civil Engineering and Geosciences, Delft University of Technology, Delft, The Netherlands.
Email: y.tang-3@tudelft.nl

Funding information
Chinese Scholarship Council; Nederlandse Organisatie voor Wetenschappelijk Onderzoek, Grant/Award Number: STW14515

Abstract

Recently, superparamagnetic silica encapsulated DNA microparticles (SiDNAFe) were designed and in various experiments used as a hydrological tracer. We investigated the effect of bed characteristics on the transport behaviour and especially the mass loss of SiDNAFe in open channel injection experiments. Hereto, a series of laboratory injection experiments were conducted with four channel bed conditions (no sediment, fine river sediment, coarse sand, and goethite-coated coarse sand) and two water qualities (tap water and Meuse water). Breakthrough curves (BTCs) were analysed and modelled. Mass loss of SiDNAFe was accounted for as a first-order decay process included in a 1-D advection and dispersion model with transient storage (OTIS). SiDNAFe BTCs could be adequately described by advection and dispersion with or without a first-order decay process. SiDNAFe mass recoveries exhibited a wide range, varying from 50% to 120% from sediment-free conditions to coarse (coated) sediment. In 6 out of 8 cases, SiDNAFe mass recovery was complete. Retention of SiDNAFe was 1–2 orders of magnitude greater than gravitational settling rates, as determined in Tang et al. (*Hydrological Processes*, e14801, 2023). We reason this was due to grain-scale hyporheic flows and coupled water-sediment-particle interactions. The dispersive behaviour of SiDNAFe generally mimicked that of NaCl tracer. We concluded that SiDNAFe can be used in tracing experiments. However, water quality and sediment characteristics may affect the fate of SiDNAFe in river environments. SiDNAFe is a promising tool for particulate multi-tracing in large rivers.

KEYWORDS
breakthrough curve, deposition, DNA, magnetic microparticle tracer, particle retention, riverbed

1 | INTRODUCTION

DNA tracers for hydrological investigations have received an increased interest over the past decade (Zhang & Huang, 2022). Synthetic DNA tracers enable multi-tracing with virtually infinite numbers of unique DNA sequences which are distinguishable from the environmental background (Liao et al., 2018). Therefore, engineered nano- or micro-particles with DNA barcodes could serve as an

alternative for particle contaminant environmental tracing, where synthetic ds/ss DNA strands are well protected from DNA degradation due to environmental stressors. To date, hydrologists have explored several engineered particle variants with DNA tags, in which DNA was encapsulated or associated with desired materials, for example, clay particles (Mahler et al., 1998), silica (Paunescu et al., 2013), iron oxides (Puddu et al., 2014; A. Sharma et al., 2021), and organic material (Garnett et al., 2009; McNew et al., 2018; Pang et al., 2020; A. N. Sharma et al., 2012). Such DNA-tagged micro-composites have been proven to be detectable and could survive significantly longer than 'naked' DNA strands for tracing small-scale surface and subsurface geographic settings (Bovolin et al., 2014; Dahlke et al., 2015; Foppen et al., 2013; McCluskey et al., 2021; Mikutis et al., 2018; Pang et al., 2020, 2022; Sabir et al., 1999). One of the main purposes of using magnetic DNA-tagged microparticles as a hydrological tracer is to be able to resolve the dilution factor and subsequently the detection limits of hydrological tracers in larger-scale hydrological systems. By collecting water samples in large volumes and subsequently applying magnetic separation to up-concentrate SiDNAFe, hydrologists could use a small amount of SiDNAFe mass (e.g., a few grams) to trace large-scale water bodies, such as big rivers. To this end, a superparamagnetic silica encapsulated DNA microparticle (SiDNAFe) was designed to be efficiently up concentrated prior to analysis (A. Sharma et al., 2021; Tang et al., 2023). The micro-sized DNA-tagged tracers seem to have more tracing potential for applications in surface water than in subsurface porous media, mainly because they are subject to filtration removal in porous media (Pang et al., 2020). Nevertheless, DNA-tagged microparticles also experience mass loss of varying degrees compared with conservative tracers in fast-flowing water environments (Kittila et al., 2019; Pang et al., 2020). To be able to design river tracing experiments with DNA-tagged tracers, quantitative analysis of the microparticle behaviour in river water and upon contact with the riverbed is a prerequisite.

In rivers, transport of waterborne constituents can be divided into two parts, a fast-flowing region where constituents are carried by the average fluid velocity and dispersive mixing, and a low-velocity region where a mass exchange occurs between the fast- and the low-flowing regions (Bencala et al., 2011; Boano et al., 2006; Briggs et al., 2009; Karwan & Saiers, 2009; Kerr et al., 2013; Paul & Hall Jr, 2002; Wagener et al., 2002). Near the riverbed is a low-velocity region and the riverbed acts as a significant sink for particle retention due to a process known as "hyporheic exchange", which traps a wide range of particles, including lightweight plastics (Drummond et al., 2020, 2022; Frei et al., 2019). Complex is the interaction between fluid motion, particulate matter being transported, and the flow within the streambed (Ho & Gelhar, 1973; Ruff & Gelhar, 1972). A shallow hyporheic flow can be induced by hydrodynamic forces when it is triggered by sand ripples, dunes, or grain clusters on a small spatial scale (Käser et al., 2013; Stonedahl et al., 2013), whereas a deeper and larger hyporheic flow is typically caused by hydrostatic forces beneath topographic features, for example, steps and cascades, riffles, and even larger meanderings (Boano et al., 2006; Revelli et al., 2008; Tonina & Buffington, 2009). Additionally, flow velocity (Elliott & Brooks, 1997; O'Connor et al., 2012), pH, temperature, chemistry of the flowing water (Ren et al., 2002; Westhoff et al., 2011), permeability and surface roughness of the streambed (e.g., biofilm) (Battin et al., 2003; Roche et al., 2017), and, finally, bed mobility (Harvey et al., 2012), working in concert, regulate the interfacial interactions where surface water overlies permeable sediments.

Colloidal particles in water columns are subject to advection, dispersion, aggregation, settling, and deposition (Besseling et al., 2017; Kooi et al., 2018; Li et al., 2019; Xu et al., 2019). Tang et al. (2023) showed that interactions with suspended particulate matter (i.e., hetero-aggregation) in river waters was an insignificant factor in first-order gravitational settling of SiDNAFe in water columns at a 30-h time scale. However, rates of fine particle deposition by hyporheic exchange could be up to hundreds of times greater than those for gravitational settling (Roche et al., 2017; Thomas, et al., 2001). For example, flat-bed grain-scale flows can induce greater particle deposition than gravity and are comparable to rippled bed particle deposition (Fries & Taghon, 2010).

Therefore, in this work, we studied the effect of channel bed sediment on the transport behaviour and mass loss of SiDNAFe in open channel injection experiments using different water qualities. Hereto, a series of laboratory injection experiments were conducted with four channel bed conditions (no sediment, fine sediment, coarse sand, and goethite-coated coarse sand) and two water qualities (tap water and natural river water). This research establishes a methodological foundation for field application of SiDNAFe in river tracing and characterizes the fate and transport of SiDNAFe in riverbeds. This draws a bottom line for applying such DNA-based tracer in future real-world river tracing experiments. With its magnetic properties and the up-concentration scheme, SiDNAFe possess promising potential as a surrogate for multi-tracing micro-contaminants (e.g., microplastics) in large rivers, which could be a promising tool for enhancing understanding of hydrological processes.

2 | MATERIALS AND METHODS

2.1 | SiDNAFe and sample analysis

SiDNAFe was prepared by the Norwegian University of Science and Technology (NTNU, Trondheim, Norway). Sharma et al. (2021) described in detail the synthesis procedure and physicochemical properties of SiDNAFe. Briefly, SiDNAFe was synthesized by silica encapsulation of iron oxide nanoparticles which had been previously bound to double-stranded DNA (67 base pairs dsDNA). To quantify SiDNAFe, dsDNA was released by dissolving the protective silica shell followed by DNA quantification using quantitative polymerase chain reaction (qPCR) (Figure 1c). Before DNA analysis, SiDNAFe was up-concentrated five times after magnetically separating the sample twice with a 16-Tube SureBeads™ Magnetic Rack (Bio-Rad Laboratories, Inc., USA) (Figure 1b), and replacing the sample fluid (i.e., tap water or river water) with MilliQ. For DNA quantification, the same protocol was used as described in Tang et al. (2023). Firstly, the silica shell of SiDNAFe was dissolved by a buffered oxide etch solution (BOE, 2.3 g of NH_4FHF (Sigma Aldrich) and 1.9 g of NH_4F (J.T. Baker)). In previous

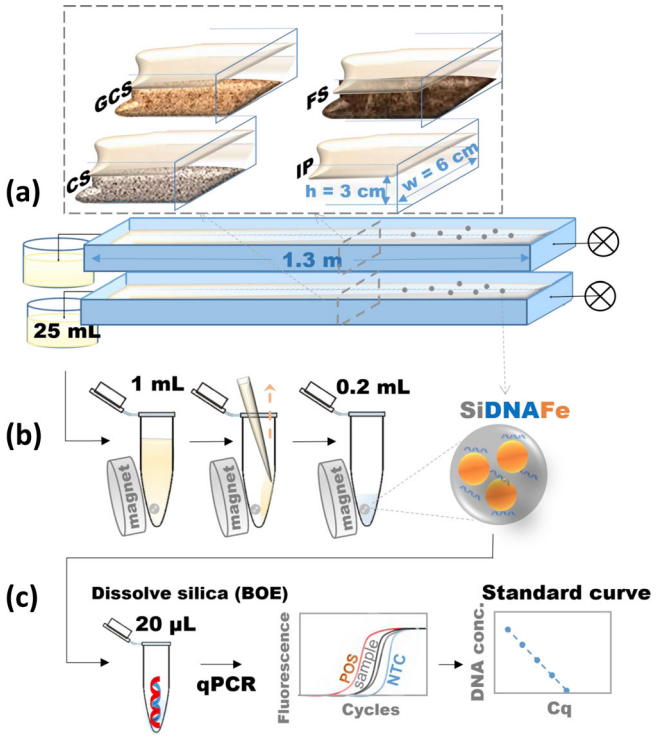

FIGURE 1 Schematic figure of open channel injection experiments and sample analysis. (a) Open channel injection experiments in duplicate: four different channel bed were tested: no sediment (IP), coarse sand (CS), goethite-coated coarse sand (GCS), and natural river fine sediment (FS), respectively (see photos in Figure S9). (b) Magnetic separation and up-concentration: 1 mL of river water or tap water was gradually diluted and replaced with MQ over two rounds of pipetting, while the SiDNAFe particles were magnetically attracted to one side of the tube. Finally, 0.2 mL of MQ was left within the tube containing the magnetically separated SiDNAFe (details shown in Figure S4a in the SI). (c) DNA analysis and sample quantification: dsDNA was released from SiDNAFe by dissolving the silica shell with BOE, and then dsDNA was amplified and quantified by qPCR with positive controls (POS) and negative controls (NTC) included in each assay. A standard curve of DNA concentrations as a function of Cq was produced in each qPCR assay for sample quantification.

studies, dilute BOE solutions have shown to dissolve both the silica shell and the iron oxide core effectively, without affecting DNA (Paunescu et al., 2013; Puddu et al., 2014). After pH adjusted with 0.1 M Tris–HCl, 5 µL of sample mixture was added to 15 µL PCR mix which consisted of 10 µL SYBR green master mix (KAPA SYBR FAST qPCR MasterMix (2X) Universal, Kapa Biosystem), 1 µL 10 µM Forward Primer, 1 µL 10 µM Reverse Primer (Biolegio B.V, Nijmegen, the Netherlands), and 3 µL qPCR water. Nucleotide sequence of dsDNA and primer sequences are given in the Supporting Information (SI) (Table S1). For contamination control and to avoid manual pipetting errors, all mixing was conducted by a QIAgility high-precision automated PCR setup (QIAgility System HEPA/UV, Cat No. /ID: 9001532).

The released and intact dsDNA was quantified using qPCR on a Bio-Rad CFX96 Touch System (96 wells), whereby the amplification of dsDNA was initiated by one-time heating at 95°C for 6 min and 40 s and followed by 42 cycles of a three-step thermal profile (20 s at 95°C, 40 s at 58°C, 35 s at 72°C). A standard curve of 10-fold dilution series was prepared from the stock SiDNAFe suspension to convert measured DNA concentrations to SiDNAFe concentrations of samples in each qPCR assay (the standard curve in Figure 1c).

The zeta potential (ζ) of SiDNAFe was obtained using a ZetaSizer Nano S (Malvern Instr., UK), whereby ζ was calculated using the Smoluchowski equation from the measured electrophoretic mobility of SiDNAFe dispersed in tap water and filtered river water (0.45-µm glassfibre filter), respectively. The hydrodynamic radius of SiDNAFe was measured using Dynamic Light Scattering (DLS) method (173° backscattering).

2.2 | Open channel injection experiments

2.2.1 | Open channel setup and the bed sediment characteristics

For the injection experiments, two small, identical, horizontally placed, open channels (PVC gutters with dimension 1.3 m L × 0.06 m W) were used in parallel (Figure 1a). Flow was generated with a peristaltic pump (Watson-Marlow pumps, Falmouth, Cornwall). A rotor was set 7 cm from the inlet to homogenize the cross-sectional concentration of the entering tracer mass with little disturbance to the flow path downstream. Through the outlet point, out-flowing water was caught by sample containers. To investigate the effect of channel bed sediment characteristics on the fate and transport behaviour of SiDNAFe during injection experiments, four types of channel bed were selected (Figure 1a): an impermeable channel bed without sediment (IP) as a control, a clean quartz coarse sand bed (CS), a goethite-coated coarse sand bed (GCS), and a natural fine sediment bed (FS), respectively. The size distribution of the used sand/sediment was obtained through wet sieving (Figure S7). The roughness k_s (mm) of the channel bed has been empirically estimated as $k_s \approx 3.5 \times D_{84}$, where D_{84} represents the grain size for the 84th percentiles of the grain size distribution (Figure S7) (Clifford et al., 1992).

For CS, 1.2–1.5 mm (average 1.36 mm) quartz sand (Figure S7) was washed sequentially with tap water, nitric acid (10% v/v), and deionized water until an Electrical Conductivity (EC) of <2 µS/cm was reached. After that, the wet sand was oven dried at 70°C overnight. After cooling down, 210 g CS was laid evenly in the open channel to form a visually uniform layer with a thickness of ~3 mm (1–2 grains, Figure 1a). Retrieved from the CS series of injection experiments, the CS was coated with Goethite (GCS) using a coating procedure adapted from Scheidegger et al. (1993) and Schwertmann and Cornell (2008) (details are in the SI) and used as channel bed sand. To determine iron concentrations, the goethite coating was dissolved by adding 1 g GCS in 50 mL 10% (v/v) HNO_3 with heating for 0.5 h, the measurements were conducted in triplicate. Total Fe concentration was 0.9 mg/g using Inductively Coupled Plasma Mass Spectrometry (ICP-MS) (Analytic Jena, Jena, Germany) (Table 1). FS was collected from a top layer (~3–5 cm) of the channel bed of Merkske river

TABLE 1 The hydrodynamic condition of the open-channel flume in open-channel injection experiments.

	A	w	Q	u	R_h	Re	Fr
Unit	cm^2	cm	cm^3/s	cm/s	cm	-	-
	7.75	6	0.83	0.1	0.9	34	3.0E−03

(51°24′57.1″ N, 4°50′48.5″ E), which is located on the border of the Netherlands and Belgium. The sediment was very homogeneous. It consisted of 80.6% fine sand (125–250 μm), 5.0% very fine sand (<125 μm), and 14.4% medium sand (250–500 μm). After acid-digestion of FS, the organic matter (OM) content of FS was measured to be ∼0.5 mg-C/g, as dissolved organic carbon (DOC, in mg-C/L) using the combustion technique with a total organic carbon analyser (TOC-VCPN (TN), Shimadzu, Japan).

2.2.2 | Flume hydrodynamics

The flow rate was set constant by a peristaltic pump (100 series cased pump 120 U, Watson-Marlow). The water depth was measured after a steady flow was reached. The mean flume velocity, u, was calculated as follows,

$$u = \frac{Q}{A} \quad (1)$$

where Q is the flow rate (cm^3/s), A is the cross-sectional area perpendicular to the flow direction (cm^2). Flume Reynolds number was calculated as,

$$\mathrm{Re} = \frac{4uR_h}{\nu} \quad (2)$$

where ν is the kinematic viscosity of water (cm^2/s), and R_h is the hydraulic radius of the channel. The Froude number was calculated as,

$$\mathrm{Fr} = \frac{u}{\sqrt{g\frac{A}{w}}} \quad (3)$$

where w is the flume width (cm), and g is the gravitational constant (cm/s^2).

2.2.3 | River water

The river water was collected in March 2021 from the Meuse at Keizersveer, The Netherlands (51°43′05.7″ N, 4°53′27.5″ E), and was stored at 4°C in polyethylene sample containers and filled and tightened with double-sealed plastic caps. The river water sample was treated with 1 ppm iodide to minimize microbial activity during sample storage. The OM content of Meuse water was measured as dissolved organic carbon (DOC, in mg-C/L) using the combustion technique with a total organic carbon analyser (TOC-VCPN (TN), Shimadzu, Japan). EC and pH were measured in situ using an EC meter (Multi 3620 IDS, Xylem Analytics Germany GmbH, Germany) and a pH meter, respectively. The total suspended solids (TSS) in river water samples were calculated by drying the filtrate (>1.2 μm) at 105°C and weighing the dry weight of the filtrate.

2.2.4 | Injection experiments

SiDNAFe injection experiments were performed in duplicate in Tap water and Meuse water, respectively. First, the sand/sediment was laid evenly across the channel. After that, Tap/Meuse water was pumped into the open channel setup until a steady outflow was reached (the volumetric flow rate, $Q = 0.83\ cm^3/s$; Table 1). At the beginning of an injection experiment, SiDNAFe was suspended in the same water type used for the injection experiment to reach a concentration of $\sim 10^{-4}$ mg/mL. Then, 45 mL of SiDNAFe suspension was pumped into the channel setup at the same flow rate as the inlet flow generated by the pump. After the tracer injection, the inlet source was immediately switched back to the water type used for the injection experiment. Meanwhile, at the outlet point of the open channel, 25 mL samples were taken according to the schedule depicted in Table S2 (in SI). For each 25-mL sample, a sub-sample of 1 mL was taken in duplicate for magnetic separation and up-concentration, and DNA quantification (Figure 1b,c). Before taking the subsample, the sample was vortexed for 1 min to ensure sample homogeneity. Breakthrough curves (BTCs) of SiDNAFe were obtained from qPCR data against a standard curve of 10-fold diluted known sample concentrations. Following an injection experiment of SiDNAFe, the sediment from the channel bed was collected and washed with deionized water to quantify any SiDNAFe previously retained. Prior to SiDNAFe injection experiments, for reference, NaCl injection experiments were performed. NaCl concentrations as a function of elapsed time were measured by an EC meter (Multi 3620 IDS, Xylem Analytics Germany GmbH, Germany). The schedule outlining the specific timing for the sequence of injection experiments can be found in Table S8 of the SI.

2.3 | Statistical tests

One-way analysis of variance (ANOVA) and then a post-hoc Tukey's Honestly-Significant Difference (Tukey HSD) test (Tukey, 1949) were performed to assess the effect of the four channel-bed sand types and the two water types on the mass recoveries of SiDNAFe in injection experiments. Data variations across different groups of bed types and in between two water types per bed type were assessed using a one-way ANOVA test and a Student t-test with Welch correction, respectively. The differences were considered significant when $p < 0.05$.

2.4 | BTC analysis and 1-D transport modelling

One-dimensional advective and dispersive transport in a main channel with transient exchange/first-order mass loss was considered to be the main transport process of SiDNAFe in the open-channel injection experiments. To assess SiDNAFe BTC characteristics, One-dimensional Transport with Inflow and Storage model (OTIS) was used for BTC fitting and transport parameter optimization (Runkel, 1998). The delayed delivery of tracer mass (i.e., the tailing effect/skewness of a BTC) was treated as a first-order transient exchange between a main channel and a lumped transient storage zone. Furthermore, in case of mass loss of SiDNAFe, an additional first-order decay process in the main channel was included in the OTIS simulation. The equations used for the conservative and non-conservative (terms in square brackets) transport in our injection experiments are:

$$\frac{\partial C}{\partial t} = -\frac{Q}{A}\frac{\partial C}{\partial x} + \frac{1}{A}\frac{\partial}{\partial x}\left(AD_L\frac{\partial C}{\partial x}\right) + \alpha(C_S - C) + [-\lambda C] \quad (4)$$

$$\frac{dC_S}{dt} = \alpha\frac{A}{A_S}(C - C_S) \quad (5)$$

where C and C_S (g/m^3) are mass concentrations in the main channel and the storage zone, respectively; Q volumetric flow rate (m^3/s), A and A_S (m^2) cross-sectional areas in the main channel and storage zone, respectively; D_L (m^2/s) longitudinal dispersion coefficient; α (1/s) storage zone exchange coefficient; t (s) transport time; x (m) distance. In case of mass loss with a negligible transient storage exchange, λ (1/s) the first-order decay coefficient in the main channel was included (in the square brackets). The hydrodynamic conditions for modelling setup are shown in Table 1.

The parameter optimization was automated using the Nonlinear Least Square (NLS) algorithms of STARPAC (see details in Donaldson & Tryon, 1987), which was implemented in OTIS-P. For the OTIS modelling, we used one master BTC curve, which was averaged from four individual observed BTCs (2 experiments; 2 samples per time-interval per experiment). Four parameters D_L, α, A, and A_S were optimized in case of conservative transport, while one more parameter λ was estimated in case of mass loss. A visual inspection of the BTCs and sensitivity analysis was performed to determine the most appropriate combinations of processes to be considered. When the transient storage parameter set (i.e., A_S and α) showed negligible sensitivity on the BTC fitting, transient storage was turned off. Mass recovery was calculated by integrating the area underneath the BTC. Due to the intrinsic variations caused by DNA amplifications in qPCR (see Tang et al. (2021) for more detailed discussion), measured mass recoveries of SiDNAFe between 80% and 120% were considered full mass recovery and were linearly scaled to 100% to balance the input and the output mass for modelling purposes. This correction does not influence the BTC characteristics (Pang et al., 2017; Tang et al., 2021). Furthermore, a first-order decay term was considered in the case of mass recovery lower than 80%. The optimized parameter sets were presented with 95% confidence intervals, whereby the statistical analyses related to the observed data and the NLS fitting procedure were conducted by STARPAC (Donaldson & Tryon, 1987).

3 | RESULTS

3.1 | Sand and SiDNAFe characteristics in tap water and Meuse water

The zeta potential (ζ) of CS, GCS, and FS ranged between −15 and −19 mV (Table 2) which was determined using a ZetaSizer Nano S (Malvern Instr., UK). To do the analysis, abrasion of the surface of CS, GCS, and FS was done by ultra-sonication. The total porosity of CS, GCS, and FS was determined gravimetrically to be 0.43, 0.46, and 0.5, respectively (Table 2).

SiDNAFe was negatively charged in MQ, Tap water, and Meuse water, with a zeta potential ranging between −22 and −24 mV. The hydrodynamic radius (R_h) of SiDNAFe was measured to be ∼444–548 nm (Table 2). With a relatively low particle concentration of ∼10^{-5} mg/mL, SiDNAFe was well-dispersed at room temperature, given its zeta potential in the ionic strength and pH of tap water and of Meuse water (Tables 2 and 3).

TABLE 2 Characteristics of FS, GCS, and CS and SiDNAFe.

	-	FS	GCS	CS	SiDNAFe	
	ζ (mV)					R_h (nm)
	MQ	-	-	-	−24 ± 3.9	444 ± 133
	Tap	−15	−19	−17	−22 ± 3.1	500 ± 164
ζ (mV)	Meuse	−15	−18	−18	−23 ± 3.5	548 ± 138
DOC (mg-C/g)	Tap	0.50	-	-	-	
	Meuse	0.48	-	-	-	
Effective size (mm)		0.18	1.36	1.36	-	
Roughness (mm)		0.77	5.32	5.32	-	
Porosity		0.5	0.46	0.43	-	
Total Fe (acid-digestion) (mg/g)		0.66	0.9	-	-	

3.2 | NaCl BTCs

NaCl BTC showed an asymmetry, with a flattening tendency from FS to GCS to CS to IP. The first arrival of NaCl was similar among four bed types (Figure 2). After the first arrival, BTCs had sharp rising limbs followed by falling limbs with a similar range of slopes. FS and GCS had the highest peaks followed by CS and IP. Half of the NaCl mass arrived before one-third of the whole BTC period (between 20 and 40 min), while the other half of the mass was gradually recovered until the end at 140 min, with a total mass recovery ranging from 94% to 99%.

3.3 | BTC comparison between SiDNAFe and NaCl

Figure 3 shows an overview of BTC comparisons between SiDNAFe and NaCl, in four channel bed types and each performed in two water types. SiDNAFe BTCs are shown as master curves, using the average of four observed BTCs (see Figure S5 for all observed

TABLE 3 Water quality characteristics of Meuse water and Tap water.

Water quality	Unit	Meuse	Tap
pH	-	8.2	8.2
EC	µS/cm	533	511
Ionic strength	mM	8.5	8.1
DOC	mg-C/L	5.0	2.4
TSS	mg/L	2.3	0.0
Na^+	mg/L	28.5	39.8
K^+	mg/L	6.6	6.7
Ca^{2+}	mg/L	73.0	51.6
Mg^{2+}	mg/L	7.8	7.4
Cl^-	mg/L	38.6	56.7
NO^{3-}	mg/L	17	10
$SO4^{2-}$	mg/L	48.0	48.0
$PO4^{3-}$	mg/L	0.8	0.0

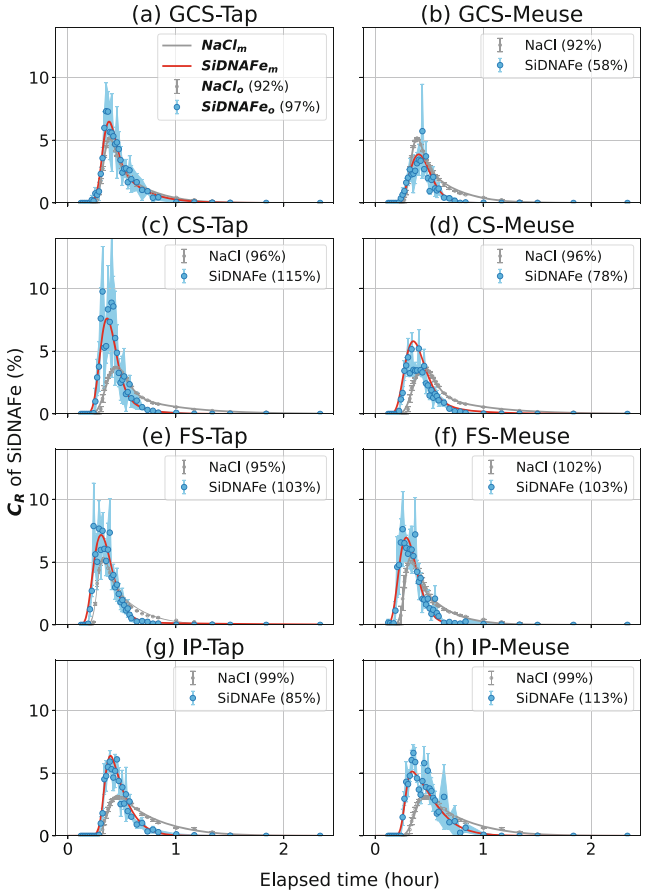

FIGURE 3 SiDNAFe BTCs in comparison with NaCl BTCs in open-channel injection experiments with four types of channel beds and two water types. BTCs are shown in relative concentrations (CR: C/C_0 in %) over time. GCS represents goethite-coated coarse sand, CS coarse sand, FS fine sediment, and IP impermeable channel without sediment. Observed SiDNAFe BTCs and OTIS-simulated SiDNAFe BTCs are shown in blue closed circles with standard deviations and red solid lines, respectively. NaCl series are shown in grey dots with standard deviations and grey solid lines. Each series of injection experiments were performed in Tap water (the left column) and in Meuse water (the right column), respectively. Mass recovery for each injection experiment is shown in brackets in each subplot. The red solid line in subplot (g) shows the simulated SiDNAFe BTC fitted with a first-order decay process in OTIS.

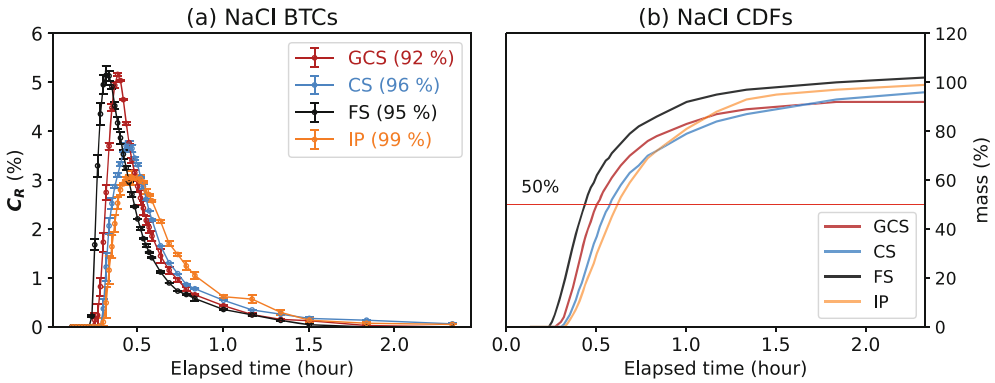

FIGURE 2 BTCs of NaCl and their corresponding cumulative distribution function (CDFs) in open channel injection experiments with four types of channel bed: fine sediment (FS), goethite-coated coarse sand (GCS), coarse sand (CS), and an impermeable channel without sediment (IP). Mass recoveries are shown in brackets. In (b), the red horizontal line denotes 50% of the recovered NaCl mass.

SiDNAFe BTCs). SiDNAFe travelled at the same rate or faster in comparison with NaCl. SiDNAFe arrived earlier than NaCl in FS series (i.e., both in Tap and in Meuse water), CS series, and IP series. However, in GCS series, SiDNAFe and NaCl arrived at the same time. SiDNAFe had a similar or steeper rising slope than NaCl after arrival. SiDNAFe concentration rose in IP series and CS series with a slope steeper than NaCl, whereas in FS and GCS series, SiDNAFe and NaCl are comparable. In all series except GCS, SiDNAFe reached a peak significantly higher than NaCl. In GCS series, SiDNAFe had a similar peak to NaCl in Tap water, but in Meuse water, SiDNAFe's peak was significantly lower due to mass loss. Additionally, SiDNAFe's peaks were characterized by discrete pulses of data points with relatively larger standard deviations. No generalized pattern was found for the extent of data scatter as a function of the channel bed types and the water types, respectively (the light blue shades of SiDNAFe BTCs in Figure 3). The falling limbs, which were quite symmetrical to the rising ones, appeared over those scattered points coming after the peak clouds in CS series, FS series, and GCS in Meuse water (hereafter referred to as GCS-Meuse). In IP series, SiDNAFe's tailing effect was evident but less pronounced than NaCl's. Further, in GCS-Tap, SiDNAFe and NaCl had almost overlapped recession curves, despite SiDNAFe having the higher standard deviations. *T*-test with Welch's correction analysis indicated that there was no statistically significant difference between the BTCs of SiDNAFe and NaCl in GCS-Tap.

3.4 | Mass recovery of SiDNAFe

Mass recoveries of SiDNAFe ranged between 54% and 135% across all channel bed types and water types (Figure 4). A Tukey post-hoc test revealed that, in Meuse water, three groups of mass recoveries (i.e., FS, GCS, and CS) were significantly different from each other ($p << 0.01$). However, in Tap water, mass recoveries of SiDNAFe were not significantly different across the four bed types we used ($p = 0.1525$).

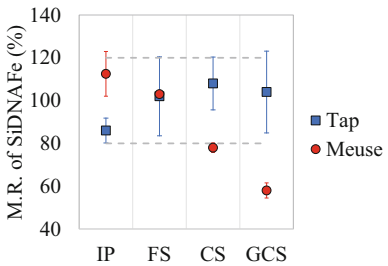

FIGURE 4 Mean mass recoveries of SiDNAFe categorized by four channel bed types: fine sediment (FS), goethite-coated coarse sand (GCS), coarse sand (CS), and an impermeable channel without sediment (IP). Blue squares and red dots denote mean mass recovery, with error bars indicating variation between four values, in Tap water and in Meuse water, respectively. The grey dashed lines delineate mass recoveries lower than 80% and higher than 120%.

3.5 | Transport parameter estimation

Figure 5 presents transport parameter estimation for SiDNAFe and NaCl with 95% confidence intervals (parameter values are presented in Table S3 in the SI). $\mathbf{D_{LNaCl}}$ varied between 1.51×10^{-5} and 2.63×10^{-5} (m^2/s), while $\boldsymbol{\alpha}_{\mathbf{NaCl}}$ varied between 4×10^{-4} and 10×10^{-4} (1/s). A trade-off between $\mathbf{D_{LNaCl}}$ and $\boldsymbol{\alpha}_{\mathbf{NaCl}}$ was observed across four bed types, where a higher $\mathbf{D_{LNaCl}}$ was correlated with a lower $\boldsymbol{\alpha}_{\mathbf{NaCl}}$ and vice versa. $\mathbf{A_S}$ the volume of sand/sediment in the channel increased from a no-sediment to a sediment-laid bed type, main channel cross-sectional area $\mathbf{A}_{\mathbf{NaCl}}$ decreased from 10×10^{-4} to 7×10^{-4} (m^2). $\mathbf{A_{SNaCl}}$ remained around half of the $\mathbf{A}_{\mathbf{NaCl}}$ in all four bed types under the same hydraulic conditions.

$\mathbf{D_{LSiDNAFe}}$ ranged between 1.07×10^{-5} and 7.97×10^{-5} (m^2/s), with FS having the greatest value, followed by GCS and CS with intermediate values, and IP with the lowest value. The transient storage exchange process was included only in the IP series and GCS-Tap, with a higher $\boldsymbol{\alpha}_{\mathbf{SiDNAFe}}$ in the IP series ($11 \times 10^{-4} \sim 20 \times 10^{-4}$ 1/s) but a lower one (6×10^{-4} 1/s) in GCS-Tap. In four bed types, $\mathbf{A}_{\mathbf{SiDNAFe}}$

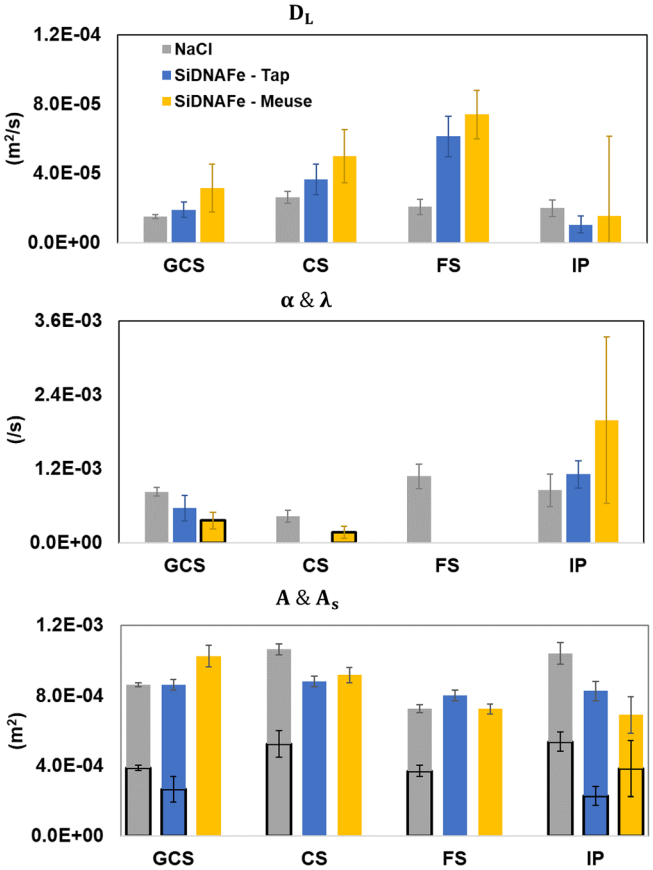

FIGURE 5 Transport parameters estimation with 95% confidence intervals for SiDNAFe and NaCl. SiDNAFe in Tap and in Meuse were shown in blue bars and yellow bars, respectively, while NaCl was shown in grey bars. λ is shown as bars with black borders in the same plot of α, and $\mathbf{A_S}$ is shown as a part of **A** (where applicable) with black borders in the subplot of **A** and $\mathbf{A_S}$. Missing bars represent no applicable parameters for this category.

was similar in Tap water ($8–9 \times 10^{-4}$ m^2), but, in Meuse water, it ranged from 7×10^{-4} to 10×10^{-4} [m^2], with the highest value in GCS and the lowest value in IP. $\mathbf{A}_{\mathbf{S}\text{SiDNAFe}}$ was estimated to be half of the $\mathbf{A}_{\text{SiDNAFe}}$ in IP-Tap but around 30% of the $\mathbf{A}_{\text{SiDNAFe}}$ in IP-Meuse and GCS-Tap when transient storage was considered. To account for the mass loss in GCS-Meuse and in CS-Meuse, a first-order decay term was included and modelled to be 3.62×10^{-4} and 1.70×10^{-4} [1/s], respectively.

When comparing NaCl and SiDNAFe, $\mathbf{D}_{\mathbf{L}\text{SiDNAFe}}$ was higher than $\mathbf{D}_{\mathbf{L}\text{NaCl}}$ in CS, FS, and GCS-Meuse. Notably, in these cases, the transient storage was turned off because the transient storage parameters could not be constrained in inverse simulations (i.e., negligible sensitivity of $\mathbf{A}_{\mathbf{S}}$ and $\boldsymbol{\alpha}$ on the BTC fitting, see details in SI). When comparing SiDNAFe and NaCl with transient storage included (i.e., IP and CS series), an equivalent or a smaller portion of A was modelled as $\mathbf{A}_{\mathbf{S}}$ to exchange mass at a similar range of $\boldsymbol{\alpha}$. Additionally, $\mathbf{A}_{\text{SiDNAFe}}$ was smaller than $\mathbf{A}_{\text{NaCl}}$ in IP and CS. On the contrary, in GCS and FS, $\mathbf{A}_{\text{SiDNAFe}}$ was either equivalent or larger than $\mathbf{A}_{\text{NaCl}}$ (i.e., in FS-Tap and GCS-Meuse). Across two water types, SiDNAFe had similar transport parameters when they were subject to the same transport processes.

4 | DISCUSSION

4.1 | The effect of channel beds

SiDNAFe mass recoveries exhibited a wide range, varying from 50% to 120% from sediment-free conditions to fine sediment and to coarse (coated) sediment conditions. SiDNAFe had mass loss in coarse (coated) sediment series, but no mass loss in the IP series. This indicated that gravitational settling was negligible in the experiments, and mass loss was likely related to interactions with the sediment. For effective particle retention, most studies found that two processes have to work in concert, that is, the particle delivery from the flow to bed, and the detainment of particles such as filtration (Fries & Taghon, 2010; Packman et al., 2000; Ren & Packman, 2004a, 2004b, 2005; Thomas, et al., 2001; Wörman et al., 2002). However, in our experiments, the effect of filtration was considered minor, due to a relatively thin layer of sediment bed of ~3 mm and the permeability of the bed (Table S4). The near-boundary shear Reynolds number for FS, GCS, and CS was calculated to be smaller than 3 (Table S4), indicating a hydraulically smooth flow condition (Nikaradse, 1933), where the laminar sublayer above the water–sediment interface was thicker than the roughness elements of the bed. Upon approaching the water–sediment interface (i.e., particle delivery), SiDNAFe, which was significantly smaller than the sublayer in size, was supposed to be entirely immersed within this viscous sublayer, where the molecular diffusion should dominate the particle transport (Crawford & Sanford, 2001). The same diffusion responsible for particle delivery also transports momentum into the sediment, driving an interstitial flow. Fries (2002) found that over a flat permeable bed such an interstitial flow can be detected as a velocity slip at the interface. This slip decreases the drag coefficient and generates a negative correlation between drag and deposition over a flat permeable bed (Fries, 2002). Moreover, the influence of slip in the boundary on the flow profile was most significant at a lower grain Reynolds number (i.e., smaller grain size or smaller shear velocity). In our experiments, the ratio of void scale to permeability of FS, GCS, and CS was similar, indicating an equivalent open structure of the sediment bed (Table S4). If a mechanism like the above-mentioned diffusive transport and filtration was in play, SiDNAFe would likely have been more deposited in FS than in CS & GCS, due to a lower grain Reynolds number in FS. From no-sediment to sediment conditions, we speculated that the retention of SiDNAFe was associated with particle exchange brought by grain-scale hyporheic flows (Packman et al., 2000; Ren & Packman, 2004a, 2004b, 2005; Wörman et al., 2002) and the nature of the boundary layer over the bed (Hamm et al., 2011; Saffman, 1965).

There was no significant difference in NaCl transport parameters among the four series, except that with the addition of sand/sediment volumes in the channel the effective main channel cross-sectional area was reduced and caused an increase in NaCl BTC peak and an earlier NaCl arrival (Figure 2). The trade-off between $\mathbf{D}_{\mathbf{L}\text{NaCl}}$ and $\boldsymbol{\alpha}_{\text{NaCl}}$ indicated that the effect of the transient storage on NaCl transport was on a similar timescale as the hydrodynamic dispersion process in our injection experiments (Briggs et al., 2009). However, there should be a difference in the nature of the transient exchange between with and without channel bed sand. In addition to the exchange between the main channel and surface transient storage where fluid moved slowly or stagnated, a grain-scale hyporheic exchange on the water–sediment interface was likely for the sand-laid cases (Fries & Taghon, 2010).

4.2 | The coupled effect of water quality and coarse sediment

We only observed SiDNAFe mass loss in coarse (coated) sediment bed conditions (i.e., GCS and CS) in Meuse river. Interestingly, this trend was not observed in Tap water under the same series of bed conditions.

The primary differences of the water quality characteristics lay in the dissolved organic carbon (DOC) and total suspended solids (TSS) content (Table 3). Prior research on the settling behaviour of SiDNAFe has demonstrated the insignificance of hetero-aggregation with suspended particulate matter (SPM) in Meuse water (Tang et al., 2023). Furthermore, the pH, ionic strength, and major cations and anions are similar for both water types. Consequently, in our experiments we expected the effect of water chemistry on the colloidal stability of SiDNAFe to be similar, that is, negligible. Given the current experimental results and water quality measurements, we were unable to conclusively pinpoint the decisive water quality factor that contributed to the observed differences in mass recovery between these two water types. While it is meaningful to delve into the controlling physicochemical characteristics behind the observed mass loss in this particular case, such an investigation requires further research. Nonetheless, our overarching message is that in real world large-scale

tracing experiments, SiDNAFe is a promising tracer albeit that in some environmental conditions the particle loss may hinder the measurement.

Specifically, SiDNAFe mass retention in coarse (coated) sediment bed conditions was 1–2 orders of magnitude greater than the estimated first-order decay rate in quiescent settling conditions (Tang et al., 2023). Similarly, Fries and Taghon (2010) found that deposition in excess of gravitational settling could result from the grain-scale deposition process of colloidal particles to permeable sediments regardless of bed roughness. Furthermore, enhanced deposition and retention of particles was associated with a greater flow-to-bed flow as a result of a local increase in pressure-driven flows and most likely followed by particle capture. However, this was not the case given the flatbed condition. Thomas, et al. (2001) found that $\frac{A_s}{A}$ was most strongly associated with the variation in enhanced deposition rates, which was consistent with interstitial filtration as a significant mechanism of particle deposition. However, in our experiments, transient exchange was negligible in the two cases where enhanced SiDNAFe mass retention occurred. This was additional indirect evidence supporting that filtration did not take place as the main mechanism of enhanced SiDNAFe mass retention in coarse (coated) sediment bed conditions.

It is reasonable to consider that there were different mechanisms than the above-mentioned, driving the enhanced mass loss in coarse (coated) sediment beds with Meuse water. We think that it was related to complex water-sediment-particle interactions. Ren and Packman (2005) found that colloid mobility could be either enhanced or reduced as a result of general and specific interactions between sorbing solutes and iron oxide particles, and they suggested that the colloidal and contaminant behaviour assessment cannot be separated from each other in surface systems because surface-chemical processes can cause their behaviour to be coupled. In this regard, we speculate that some sort of coupled grain-scale water-sediment-particle interactions, for example, kinetic attachment between SiDNAFe and surface heterogeneities of coarse (coated) sediment in the presence of river water were the driving mechanism for enhanced SiDNAFe retention. Moreover, kinetic attachment/detachment was concluded to be the driving deposition mechanism in porous media for a similar silica encapsulated DNA microparticles (Kianfar et al., 2022). Another indirect evidence supporting this was the lower mass loss in CS, which was acid-washed and removed from surface impurities. Compared with the surface heterogeneities of GCS, CS would have weaker particle-particle interactions with SiDNAFe. Likewise, Ren et al. (2002) showed a reduced deposition of silica colloids in a sand bed that was acid- and base-washed. Mechanisms that would otherwise enhance the retention, such as topography and aggregation seemed unlikely, due to a flatbed condition and the constant hydrodynamic radius of SiDNAFe under similar conditions. Moreover, diffusion across the interface seemed unlikely, as the hydrodynamic dispersion was 10 to 11 orders greater than the diffusion coefficients of SiDNAFe. Only in conditions of quiescent waters with extremely low permeability sediments (clays or silts) does diffusion tend to be the dominant transport process (Huettel & Webster, 2001). In our experiments, SiDNAFe would likely attach to or be deposited on the grain surfaces. Despite the unfavourable conditions for attachment between SiDNAFe and coarse (coated) sediment, enhanced deposition could occur as a result of grain-scale surface heterogeneity (Ryan & Elimelech, 1996; Schijven et al., 2002), which had been shown to be responsible for a considerable amount of the particle retention which occurred under repulsive electrostatic forces (Ren et al., 2002).

4.3 | Comparison between NaCl and SiDNAFe

An evident breakthrough separation was between NaCl and SiNDAFe in IP, CS, and FS, despite the more "chaotic" signals of SiNDAFe. In IP and CS, SiDNAFe arrived slightly earlier than NaCl in both Tap and Meuse water conditions. This indicated that the average velocity of SiDNAFe was higher than that of NaCl. In many surface water tracer experiments, researchers have observed the earlier arrival of the BTC peak by colloids compared to solute tracers (e.g., Göppert & Goldscheider, 2008; McCluskey et al., 2021). This suggests that colloids tend to preferentially travel along faster flow lines in comparison to solutes. However, it is important to note that these differences are generally small, as also observed in our own experiments, and are primarily noticeable at lower average flow velocities (Göppert & Goldscheider, 2008). In FS, despite an earlier arrival of SiDNAFe, $\mathbf{A}_{\mathrm{SiDNAFe}}$ was estimated to be similar to $\mathbf{A}_{\mathrm{NaCl}}$. This was probably because a significantly higher $\mathbf{D}_{\mathrm{LSiDNAFe}}$ accounted for an earlier arrival in this case. However, we argue that a significantly greater $\mathbf{D}_{\mathrm{LSiDNAFe}}$ was a result of modelling compensation. OTIS model would tend to increase $\mathbf{D}_{\mathrm{L}}$ to compensate for the effect of the transient exchange when the transient storage parameters failed to constrain the simulation (Karwan & Saiers, 2009). This also indicated that the effect of the transient exchange of transport was on a similar time scale as the dispersion process, which corresponds to the trade-off effect shown earlier between $\mathbf{D}_{\mathrm{LNaCl}}$ and $\boldsymbol{\alpha}_{\mathrm{NaCl}}$ in NaCl BTC simulations.

However, in GCS-Tap, SiDNAFe behaved almost identically to NaCl. In addition, SiDNAFe and NaCl arrived at the same time, showing a symmetric BTC in GCS-Meuse. This change indicated that sediment coating and surface heterogeneity could increase the transient interactions with the particles.

4.4 | Advantages of SiDNAFe and its associated uncertainty

There was no significant difference between standard deviations of SiDNAFe concentrations ($\boldsymbol{\sigma}_{\mathrm{SiDNAFe}}$) in Tap water and in Meuse water at a 95% significance level ($p = 0.5864$). In addition, no significant difference was found among $\boldsymbol{\sigma}_{\mathrm{SiDNAFe}}$ grouped by different sediment conditions (i.e., FS, GCS, CS, IP). The 'noise' was more associated with the lower concentrations (rising limbs and tails) rather than the higher concentrations (peaks) (Figure 6). Most of the coefficient of variation

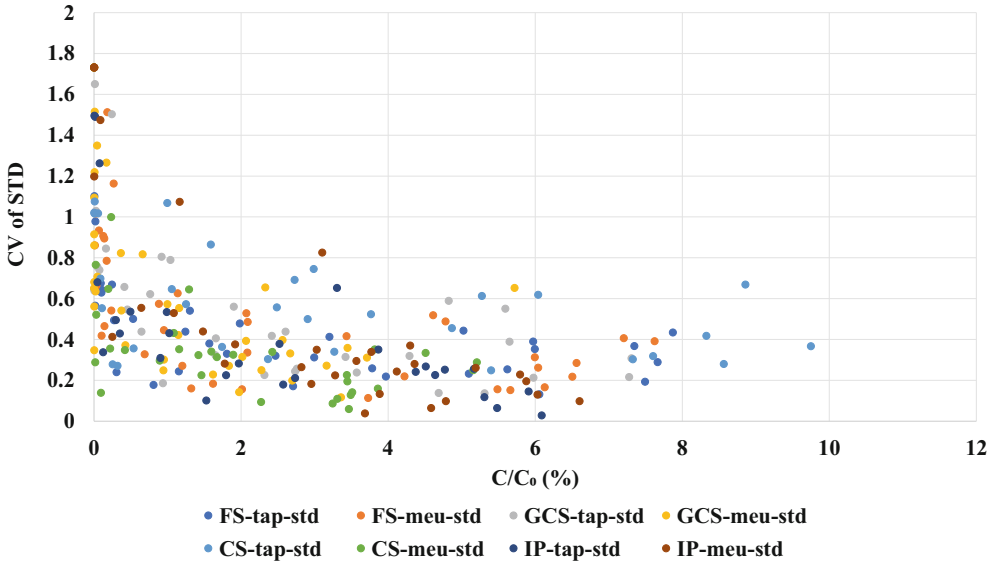

FIGURE 6 Coefficient of variations (CV) of the standard deviation of SiDNAFe concentrations ($\sigma_{SiDNAFe}$) as a function of relative concentration C/C_0 (%).

(**CV**) were lower than 0.6. However, when the C/C_0 was below 1%, the **CV** ranged between 0 and 1.8, indicating a high uncertainty of the concentration value. This high uncertainty of lower concentration was due to having only a few particles/DNA molecules present in the sample for DNA quantification. This range of CVs was consistent with our previous experimental results on the **CV** of DNA-tagged tracer BTC (Tang et al., 2021). Further, no generic pattern was found for the significant difference of σ_{RC} and its **CV** by comparing between groups of channel beds and water types (details in SI). As discussed in Tang et al., 2021 and other DNA-tagged microparticle tracer application experiments (Foppen et al., 2013; Kittilä et al., 2019; Liao et al., 2018), data variation and uncertainty was mostly bound with its discrete nature of colloidal behaviour and qPCR reading uncertainties, water chemistry, etc. In this research, we also assessed the influence of magnetic separation on particle concentrations. There was no statistically significant difference across the Cq values of samples after up to five times of magnetic separation ($p = 0.4806$, see Figure S2). Additionally, Cq values of SiDNAFe suspended in tap water were not significantly different from those in Meuse water after up to five times of magnetic separation ($p = 0.6179$, Figure S2). We finalized the up-concentration protocol which was two times of magnetic separation, followed by one time of magnetic separation where one-fifth of the original volume of water was left to the sample tube to realize up-concentration. After this magnetic separation and up-concentration procedure, the slopes and R^2 of the 10-fold dilution curves of SiDNAFe, which was originally suspended in Tap water and in Meuse water, revealed that this procedure can be reliably applied to up-concentrate SiDNAFe (see Figure S3). This can help to minimize possible inhibition associated with varied river water quality for qPCR quantification.

Our results demonstrated that SiDNAFe could be used in tracing experiments, as evidenced by the complete mass recoveries observed in 6 out of 8 cases. However, apparently, certain combinations of water and sediment can lead to mass loss, as evidenced by our Meuse water-iron coated sand experiments. Here, more detailed research is recommended. Extrapolating our results to tracing experiments in real river experiments, SiDNAFe seems to have the potential to be employed as a tracer also at kilometre scale.

5 | CONCLUSIONS

We investigated the effect of the channel bed characteristics on the transport behaviour and mass loss of magnetic silica encapsulated DNA microparticle (SiDNAFe) as a colloidal tracer. Natural river fine sediment, coarse sand, Goethite-coated coarse sand, and no-sediment were used as four different channel beds. We tested SiDNAFe in two different water qualities (i.e., tap water and river water) and compared SiDNAFe to dissolved NaCl by conducting pulse injection experiments. SiDNAFe BTCs could be adequately described by advection and dispersion with or without a first-order decay process. SiDNAFe mass recoveries exhibited a wide range, varying from 50% to 120% from sediment-free conditions to coarse (coated) sediment. In 6 out of 8 cases, SiDNAFe mass recovery was complete. Retention of SiDNAFe was 1–2 orders of magnitude greater than gravitational settling rates, as determined in Tang et al. 2023. We reason this was due to grain-scale hyporheic flows and coupled water-sediment-particle interactions. The dispersive behaviour of SiDNAFe generally mimicked that of NaCl tracer. SiDNAFe can be used in tracing experiments. However, water quality and sediment characteristics may affect the fate of SiDNAFe in river environments. With its magnetic properties and the up-concentration scheme, SiDNAFe possess promising potential as a surrogate for multi-tracing micro-contaminants (e.g., microplastics) in large rivers, which could be a promising tool for enhancing understanding of hydrological processes.

ACKNOWLEDGEMENTS

Financial support was provided by the Netherlands Organization for Scientific Research (NWO) Grant STW14515 WaterTagging and by

China Scholarship Council (CSC). We would like to thank Ph.D. student Zeeshan Ali and Dr. Sulalit Bandyopadhyay from Norwegian University of Science and Technology for the synthesis of SiDNAFe tracers and fruitful scientific discussions. We would like to thank the lab staff from TUDelft Waterlab and IHE Delft for their technical and laboratory support.

DATA AVAILABILITY STATEMENT

The data that support the findings of this study are available from the corresponding author upon reasonable request.

ORCID

Yuchen Tang https://orcid.org/0000-0002-1632-4339

REFERENCES

Battin, T. J., Kaplan, L. A., Denis Newbold, J., & Hansen, C. M. E. (2003). Contributions of microbial biofilms to ecosystem processes in stream mesocosms. *Nature*, *426*(6965), 439–442.

Bencala, K. E., Gooseff, M. N., & Kimball, B. A. (2011). Rethinking hyporheic flow and transient storage to advance understanding of stream-catchment connections. *Water Resources Research*, *47*(March), 1–9. https://doi.org/10.1029/2010WR010066

Besseling, E., Quik, J. T. K., Sun, M., & Koelmans, A. A. (2017). Fate of nano- and microplastic in freshwater systems: A modeling study. *Environmental Pollution*, *220*, 540–548. https://doi.org/10.1016/j.envpol.2016.10.001

Boano, F., Camporeale, C., Revelli, R., & Ridolfi, L. (2006), Sinuosity-driven hyporheic exchange in meandering rivers, *Geophysical Research Letters*, *33*, L18406. https://doi.org/10.1029/2006GL027630

Bovolin, V., Cuomo, A., Guida, D., & Foppen, J. W. (2014). Using artificial DNA as tracer in a bed-rock river of the Middle Bussento Karst System (Cilento, Vallo Diano and Alburni European & Global Geopark, Southern Italy). June Proceedings of the 7th International Conference on Engineering Mechanics, Structures. *Engineering Geology (EMESEG'14), Salerno, 3−5 June, 2014*, pp. 105–112.

Briggs, M. A., Gooseff, M. N., Arp, C. D., & Baker, M. A. (2009). A method for estimating surface transient storage parameters for streams with concurrent hyporheic storage. *Water Resources Research*, *45*, W00D27. https://doi.org/10.1029/2008WR006959

Clifford, N. J., Robert, A., & Richards, K. S. (1992). Estimation of flow resistance in gravel-bedded rivers: A physical explanation of the multiplier of roughness length. *Earth Surface Processes and Landforms*, *17*(2), 111–126.

Crawford, S. M., & Sanford, L. P. (2001). Boundary shear velocities and fluxes in the MEERC experimental ecosystems. *Marine Ecology Progress Series*, *210*, 1–12. https://doi.org/10.3354/meps210001

Dahlke, H. E., Williamson, A. G., Georgakakos, C., Leung, S., Sharma, A. N., Lyon, S. W., & Walter, M. T. (2015). Using concurrent DNA tracer injections to infer glacial flow pathways. *Hydrological Processes*, *29*(25), 5257–5274. https://doi.org/10.1002/hyp.10679

Donaldson, J. R., & Tryon, P. V. (1987). *User's guide to STARPAC, the standards time series and regression package*. Scientific Computing Division, National Center for Atmospheric Research.

Drummond, J. D., Nel, H. A., Packman, A. I., & Krause, S. (2020). Significance of Hyporheic exchange for predicting microplastic fate in rivers. *Environmental Science and Technology Letters*, *7*(10), 727–732. https://doi.org/10.1021/acs.estlett.0c00595

Drummond, J. D., Schneidewind, U., Li, A., Hoellein, T. J., Krause, S., & Packman, A. I. (2022). Microplastic accumulation in riverbed sediment via hyporheic exchange from headwaters to mainstems. *Science Advances*, *8*(2), eabi9305. https://www.science.org

Elliott, A. H., & Brooks, N. H. (1997). Transfer of nonsorbing solutes to a streambed with bed forms: Theory. *Water Resources Research*, *33*(1), 123–136.

Foppen, J. W., Seopa, J., Bakobie, N., & Bogaard, T. (2013). Development of a methodology for the application of synthetic DNA in stream tracer injection experiments. *Water Resources Research*, *49*(9), 5369–5380. https://doi.org/10.1002/wrcr.20438

Frei, S., Piehl, S., Gilfedder, B. S., Löder, M. G. J., Krutzke, J., Wilhelm, L., & Laforsch, C. (2019). Occurence of microplastics in the hyporheic zone of rivers. *Scientific Reports*, *9*(1), 15256. https://doi.org/10.1038/s41598-019-51741-5

Fries, J. S. (2002). *Enhancement of fine particle deposition to permeable sediments*. Massachusetts Inst of Tech Cambridge.

Fries, J. S., & Taghon, G. L. (2010). Particle fluxes into permeable sediments: Comparison of mechanisms mediating deposition. *Journal of Hydraulic Engineering*, *136*(4), 214–221. https://doi.org/10.1061/(asce)hy.1943-7900.0000169

Garnett, M. C., Ferruti, P., Ranucci, E., Suardi, M. A., Heyde, M., & Sleat, R. (2009). Sterically stabilized self-assembling reversibly cross-linked polyelectrolyte complexes with nucleic acids for environmental and medical applications. *Biochemical Society Transactions*, *37*(4), 713–716. https://doi.org/10.1042/BST0370713

Göppert, N., & Goldscheider, N. (2008). Solute and colloid transport in karst conduits under low-and high-flow conditions. *Groundwater*, *46*(1), 61–68.

Hamm, N. T., Dade, W. B., & Renshaw, C. E. (2011). Fine particle deposition to porous beds. *Water Resources Research*, *47*, W11508. https://doi.org/10.1029/2010WR010295

Harvey, J. W., Drummond, J. D., Martin, R. L., McPhillips, L. E., Packman, A. I., Jerolmack, D. J., Stonedahl, S. H., Aubeneau, A. F., Sawyer, A. H., Larsen, L. G., & Tobias, C. R. (2012). Hydrogeomorphology of the hyporheic zone: Stream solute and fine particle interactions with a dynamic streambed. *Journal of Geophysical Research: Biogeosciences*, *117*(4), 1–20. https://doi.org/10.1029/2012JG002043

Ho, R. T., & Gelhar, L. W. (1973). Turbulent flow with wavy permeable boundaries. *Journal of Fluid Mechanics*, *58*(2), 403–414. https://doi.org/10.1017/S0022112073002661

Huettel, M., & Webster, I. T. (2001). Porewater flow in permeable sediments. *The Benthic Boundary Layer: Transport Processes and Biogeochemistry*, *144*, 177.

Karwan, D. L., & Saiers, J. E. (2009). Influences of seasonal flow regime on the fate and transport of fine particles and a dissolved solute in a New England stream. *Water Resources Research*, *45*(11), 1–9. https://doi.org/10.1029/2009WR008077

Käser, D. H., Binley, A., & Heathwaite, A. L. (2013). On the importance of considering channel microforms in groundwater models of hyporheic exchange. *River Research and Applications*, *29*(4), 528–535.

Kerr, P. C., Gooseff, M. N., & Bolster, D. (2013). The significance of model structure in one-dimensional stream solute transport models with multiple transient storage zones—Competing vs. nested arrangements. *Journal of Hydrology*, *497*, 133–144. https://doi.org/10.1016/j.jhydrol.2013.05.013

Kianfar, B., Tian, J., Rozemeijer, J., van der Zaan, B., Bogaard, T. A., & Foppen, J. W. (2022). Transport characteristics of DNA-tagged silica colloids as a colloidal tracer in saturated sand columns; role of solution chemistry, flow velocity, and sand grain size. *Journal of Contaminant Hydrology*, *246*, 103954. https://doi.org/10.1016/j.jconhyd.2022.103954

Kittilä, A., Jalali, M. R., Evans, K. F., Willmann, M., Saar, M. O., & Kong, X. Z. (2019). Field comparison of DNA-labeled nanoparticle and solute tracer transport in a fractured crystalline rock. *Water Resources Research*, *55*(8), 6577–6595. https://doi.org/10.1029/2019WR025021

Kooi, M., Besseling, E., Kroeze, C., van Wezel, A. P., & Koelmans, A. A. (2018). Modeling the fate and transport of plastic debris in

freshwaters. *Review and Guidance*, 58, 125–152. https://doi.org/10.1007/978-3-319-61615-5

Li, Y., Wang, X., Fu, W., Xia, X., Liu, C., Min, J., Zhang, W., & Crittenden, J. C. (2019). Interactions between nano/micro plastics and suspended sediment in water: Implications on aggregation and settling. *Water Research*, *161*, 486–495. https://doi.org/10.1016/j.watres.2019.06.018

Liao, R., Yang, P., Wu, W., Luo, D., & Yang, D. (2018). A DNA tracer system for hydrological environment investigations. *Environmental Science and Technology*, *52*(4), 1695–1703. https://doi.org/10.1021/acs.est.7b02928

Mahler, B. J., Matthew, W., Philip, B., & Hillis, D. M. (1998). DNA-labeled clay: A sensitive new method for tracing particle transport. *Geology*, *26*(9), 831–834. https://doi.org/10.1130/0091-7613(1998)026<0831:DLCASN>2.3.CO;2

McCluskey, J., Flores, M. E., Hinojosa, J., Jafarzadeh, A., Moghadam, S. V., Phan, D. C., Green, R. T., & Kapoor, V. (2021). Tracking water with synthetic DNA tracers using droplet digital PCR. *ACS ES&T Water*, *1*, 1177–1183. https://doi.org/10.1021/acsestwater.0c00245

McNew, C. P., Wang, C., Walter, M. T., & Dahlke, H. E. (2018). Fabrication, detection, and analysis of DNA-labeled PLGA particles for environmental transport studies. *Journal of Colloid and Interface Science*, *526*, 207–219. https://doi.org/10.1016/j.jcis.2018.04.059

Mikutis, G., Deuber, C. A., Schmid, L., Kittila, A., Lobsiger, N., Puddu, M., Asgeirsson, D. O., Grass, R. N., Saar, M. O., & Stark, W. J. (2018). Silica-encapsulated DNA-based tracers for aquifer characterization. *Environmental Science & Technology*. *52*(21), 12142–12152. https://doi.org/10.1021/acs.est.8b03285

Nikuradse, J. (1933). Strömungsgesetze in Rauhen Rohren. *Forschungsheft Auf Dem Gebiete Des Ingenieurwesens*, *361*(B4), 361.

O'Connor, B. L., Harvey, J. W., & McPhillips, L. E. (2012). Thresholds of flow-induced bed disturbances and their effects on stream metabolism in an agricultural river. *Water Resources Research*, *48*(8), W08504.

Packman, A. I., Brooks, N. H., & Morgan, J. J. (2000). Kaolinite exchange between a stream and streambed: Laboratory experiments and validation of a colloid transport model. *Water Resources Research*, *36*(8), 2363–2372. https://doi.org/10.1029/2000WR900058

Pang, L., Abeysekera, G., Hanning, K., Premaratne, A., Robson, B., Abraham, P., Sutton, R., Hanson, C., Hadfield, J., Heiligenthal, L., Stone, D., McBeth, K., & Billington, C. (2020). Water tracking in surface water, groundwater and soils using free and alginate-chitosan encapsulated synthetic DNA tracers. *Water Research*, *184*, 116192. https://doi.org/10.1016/j.watres.2020.116192

Pang, L., Heiligenthal, L., Premaratne, A., Hanning, K. R., Abraham, P., Sutton, R., Hadfield, J., & Billington, C. (2022). Degradation and adsorption of synthetic DNA water tracers in environmental matrices. *Science of the Total Environment*, *844*, 157146. https://doi.org/10.1016/j.scitotenv.2022.157146

Pang, L., Robson, B., Farkas, K., McGill, E., Varsani, A., Gillot, L., Li, J., & Abraham, P. (2017). Tracking effluent discharges in undisturbed stony soil and alluvial gravel aquifer using synthetic DNA tracers. *Science of the Total Environment*, *592*, 144–152. https://doi.org/10.1016/j.scitotenv.2017.03.072

Paul, M. J., & Hall, R. O., Jr. (2002). Particle transport and transient storage along a stream-size gradient in the Hubbard brook experimental Forest. *Journal of the North American Benthological Society*, *21*(2), 195–205.

Paunescu, D., Puddu, M., Soellner, J. O., Stoessel, P. R., & Grass, R. N. (2013). Reversible DNA encapsulation in silica to produce ROS-resistant and heat-resistant synthetic DNA'fossils'. *Nature Protocols*, *8*(12), 2440–2448.

Puddu, M., Paunescu, D., Stark, W. J., & Grass, R. N. (2014). Magnetically recoverable, thermostable, hydrophobic DNA/silica encapsulates and their application as invisible oil tags. *ACS Nano*, *8*(3), 2677–2685.

Ren, J., & Packman, A. I. (2004a). Stream-subsurface exchange of zinc in the presence of silica and kaolinite colloids. *Environmental Science and Technology*, *38*(24), 6571–6581. https://doi.org/10.1021/es035090x

Ren, J., & Packman, A. I. (2004b). Modeling of simultaneous exchange of colloids and sorbing contaminants between streams and streambeds. *Environmental Science and Technology*, *38*(10), 2901–2911. https://doi.org/10.1021/es034852l

Ren, J., & Packman, A. I. (2005). Coupled stream-subsurface exchange of colloidal hematite and dissolved zinc, copper, and phosphate. *Environmental Science and Technology*, *39*(17), 6387–6394. https://doi.org/10.1021/es050168q

Ren, J., Packman, A. I., & Asce, A. M. (2002). Effects of background water composition on stream-subsurface exchange of submicron colloids. *Journal of Environmental Engineering*, *128*(7), 624–634. https://doi.org/10.1061/(ASCE)0733-9372(2002)128:7(624)

Revelli, R., Boano, F., Camporeale, C., & Ridolfi, L. (2008). Intra-meander hyporheic flow in alluvial rivers. *Water Resources Research*, *44*(12), W12428.

Roche, K. R., Drummond, J. D., Boano, F., Packman, A. I., Battin, T. J., & Hunter, W. R. (2017). Benthic biofilm controls on fine particle dynamics in streams. *Water Resources Research*, *53*(1), 222–236. https://doi.org/10.1002/2016WR019041

Ruff, J. F., & Gelhar, L. W. (1972). Turbulent shear flow in porous boundary. *Journal of the Engineering Mechanics Division*, *98*(4), 975–991. https://doi.org/10.1061/JMCEA3.0003524

Runkel, R. L. (1998). *One-dimensional transport with inflow and storage (OTIS): A solute transport model for streams and rivers* (Vol. 98, No. 4018). US Department of the Interior, US Geological Survey.

Ryan, J. N., & Elimelech, M. (1996). Colloid mobilization and transport in groundwater. *Colloids and Surfaces A: Physicochemical and Engineering Aspects*, *107*, 1–56.

Sabir, I. H., Torgersen, J., Haldorsen, S., & Aleström, P. (1999). DNA tracers with information capacity and high detection sensitivity tested in groundwater studies. *Hydrogeology Journal*, *7*(3), 264–272. https://doi.org/10.1007/s100400050200

Saffman, P. G. (1965). The lift on a small sphere in a slow shear flow. *Journal of Fluid Mechanics*, *22*(2), 385–400.

Scheidegger, A., Borkovec, M., & Sticher, H. (1993). Coating of silica sand with goethite: Preparation and analytical identification. *Geoderma*, *58*, 43–65.

Schijven, J. F., Hassanizadeh, S. M., & De Bruin, R. H. (2002). Two-site kinetic modeling of bacteriophages transport through columns of saturated dune sand. *Journal of Contaminant Hydrology*, *57*(3–4), 259–279.

Schwertmann, U., & Cornell, R. M. (2008). *Iron oxides in the laboratory: Preparation and characterization*. John Wiley & Sons.

Sharma, A., Foppen, J. W., Banerjee, A., Sawssen, S., Bachhar, N., Peddis, D., & Bandyopadhyay, S. (2021). Magnetic nanoparticles to unique DNA tracers: Effect of functionalization on Physico-chemical properties. *Nanoscale Research Letters*, *16*(1), 24. https://doi.org/10.1186/s11671-021-03483-5

Sharma, A. N., Luo, D., & Walter, M. T. (2012). Hydrological tracers using nanobiotechnology: Proof of concept. *Environmental Science and Technology*, *46*(16), 8928–8936. https://doi.org/10.1021/es301561q

Stonedahl, S. H., Harvey, J. W., & Packman, A. I. (2013). Interactions between hyporheic flow produced by stream meanders, bars, and dunes. *Water Resources Research*, *49*(9), 5450–5461.

Tang, Y., Foppen, J. W., & Bogaard, T. A. (2021). Transport of silica encapsulated DNA microparticles in controlled instantaneous injection open channel experiments. *Journal of Contaminant Hydrology*, *242*, 103880.

Tang, Y., Zhang, F., Bogaard, T., Chassagne, C., Ali, Z., Bandyopadhyay, S., & Foppen, J. W. (2023). Settling of superparamagnetic silica encapsulated DNA microparticles in river water. *Hydrological Processes*, *37*(1), e14801.

Thomas, S. A., Newbold, J. D., Monaghan, M. T., Minshall, G. W., Georgian, T., & Cushing, C. E. (2001). The influence of particle size on seston deposition in streams. *Limnology and Oceanography*, *46*(6), 1415–1424.

Tonina, D., & Buffington, J. M. (2009). Hyporheic exchange in mountain rivers I: Mechanics and environmental effects. *Geography Compass*, *3*(3), 1063–1086.

Tukey, J. W. (1949). Comparing individual means in the analysis of variance. *Biometrics*, *5*, 99–114.

Wagener, T., Camacho, L. A., & Wheater, H. S. (2002). Dynamic identifiability analysis of the transient storage model for solute transport in rivers. *Journal of Hydroinformatics*, *4*(3), 199–211.

Westhoff, M. C., Gooseff, M. N., Bogaard, T. A., & Savenije, H. H. G. (2011). Quantifying hyporheic exchange at high spatial resolution using natural temperature variations along a first-order stream. *Water Resources Research*, *47*(10), W10508.

Wörman, A., Packman, A. I., Johansson, H., & Jonsson, K. (2002). Effect of flow-induced exchange in hyporheic zones on longitudinal transport of solutes in streams and rivers. *Water Resources Research*, *38*(1), 2-1.

Xu, N., Huangfu, X., Li, Z., Wu, Z., Li, D., & Zhang, M. (2019). Nanoaggregates of silica with kaolinite and montmorillonite: Sedimentation and transport. *Science of the Total Environment*, *669*, 893–902. https://doi.org/10.1016/j.scitotenv.2019.03.099

Zhang, Y., & Huang, T. (2022). DNA-based tracers for the characterization of hydrogeological systems—Recent advances and new Frontiers. *Water*, *14*(21), 3545. https://doi.org/10.3390/w14213545

SUPPORTING INFORMATION

Additional supporting information can be found online in the Supporting Information section at the end of this article.

How to cite this article: Tang, Y., van Rhijn, F., Abdelrady, A., Foppen, J. W., & Bogaard, T. (2023). Effect of channel bed sediment on the transport behaviour of superparamagnetic silica encapsulated DNA microparticles in open channel injection experiments. *Hydrological Processes*, *37*(9), e14962. https://doi.org/10.1002/hyp.14962